Mon. Not. R. Astron. Soc. **000**, 000–000 (0000) Printed 12 July 2011 (MN LATEX style file v2.2)

Where will supersymmetric dark matter first be seen?

L. Gao,[1,2⋆], C. S. Frenk[2], A. Jenkins[2], V. Springel[3,4], S. D. M. White[5]
[1]*Partner Group of the Max Planck Institute for Astrophysics, National Astronomical Observatories, Chinese Academy of Sciences, Beijing, 100012, China*
[2]*Institute of Computational Cosmology, Department of Physics, University of Durham, Science Laboratories, South Road, Durham DH1 3LE*
[3]*Heidelberger Institut für Theoretische Studien, Schloss-Wolfsbrunnenweg 35, 69118 Heidelberg, Germany*
[4]*Zentrum für Astronomie der Universität Heidelberg, Astronomisches Recheninstitut, Mönchhofstr. 12-14, 69120 Heidelberg, Germany*
[5]*Max-Planck Institute for Astrophysics, Karl-Schwarzschild Str. 1, D-85748, Garching, Germany*

12 July 2011

ABSTRACT
If the dark matter consists of supersymmetric particles, γ-ray observatories such as the Fermi satellite may detect annihilation radiation from the haloes of galaxies and galaxy clusters. Much recent effort has been devoted to searching for this signal around the Milky Way's dwarf satellites. Using a new suite of high-resolution simulations of galaxy cluster haloes (the Phoenix Project), together with the Aquarius simulations of Milky-Way-like galaxy haloes, we show that higher signal-to-noise and equally clean signals are, in fact, predicted to come from nearby rich galaxy clusters. Most of the cluster emission is produced by small subhaloes with masses less than that of the Sun. The large range of mass scales covered by our two sets of simulations allows us to deduce a physically motivated extrapolation to these small (and unresolved) masses. Since tidal effects destroy subhaloes in the dense inner regions of haloes, most cluster emission is then predicted to come from large radii, implying that the nearest and brightest systems should be much more extended than Fermi's angular resolution limit. The most promising targets for detection are clusters such as Coma and Fornax, but detection algorithms must be tuned to the predicted profile of the emission if they are to maximize the chance of finding this weak signal.

Key words: methods: N-body simulations – methods: numerical – dark matter – galaxies: haloes

1 INTRODUCTION

Annihilation radiation at γ-ray frequencies offers one of the most exciting prospects for non-gravitational detection of cold dark matter, and is expected if it consists of supersymmetric particles (e.g. Berezinsky et al. 1994, 2003; Bergström et al. 1998; Stoehr et al. 2003; Koushiappas et al. 2004; Colafrancesco et al. 2007; Diemand et al. 2007; Kuhlen et al. 2008; Pieri et al. 2008; Springel et al. 2008a; Strigari et al. 2008; Jeltema et al. 2009; Ackermann et al. 2010; Zavala et al. 2010). Much effort is being devoted to searching for this signal around the Milky Way's dwarf companions, in particular using the Fermi satellite (Abdo et al. 2010).

Predictions for the properties of the annihilation radiation rely on a detailed understanding of the structure of cold dark matter haloes which can be gained only through high-resolution numerical simulations of halo formation. The structure of galaxy-mass cold dark matter haloes has been investigated in considerable depth (e.g. Diemand et al. 2007, 2008; Kuhlen et al. 2008; Springel et al. 2008a,b; Anderson et al. 2010; Kamionkowski et al. 2010) showing that the radial distribution of low-mass subhaloes, and thus of annihilation radiation, is much less centrally concentrated than that of the dark matter as a whole. In the Milky Way, this results in the dominant subhalo contribution to the annihilation radiation coming from large galactrocentric distance and so appearing almost uniform across the sky to an observer on Earth (Springel et al. 2008a). This same effect causes the annihilation radiation from an external galaxy cluster to appear much less centrally concentrated than the distribution of galaxies. As we show below, this has significant implications for the optimal strategy for detecting the annihilation signal.

In this paper we present some of the largest high-resolution simulations of cluster haloes to date (the Phoenix Project) and use them to investigate the detailed structure of the dark matter distribution in clusters and its halo-to-halo variation. We use these data, together with data from the Aquarius set of galaxy halo simulations (Springel et al. 2008b) to predict the expected γ-ray annihilation radiation from cluster haloes which we compare to the expected annihilation radiation from giant and satellite galaxy haloes.

As we were completing this work, Pinzke et al. (2011) posted

⋆ Email:lgao@bao.ac.cn

a preprint investigating, amongst other things, the γ-ray annihilation radiation expected from galaxy clusters. The luminosity and spatial distribution of this radiation depend sensitively on the properties of surviving dark matter subhaloes down to the limiting mass of the cold dark matter power spectrum, which may be in the range 10^{-6} to $10^{-12}M_{\odot}$ (Hofmann et al. 2001; Green et al. 2005). For their analysis, Pinzke et al. (2011) relied on an extrapolation of scalings based on published results for simulations of galactic dark matter haloes, including those of the Aquarius Project. Combining the Phoenix and Aquarius simulations we test explicitly the validity of these scalings, we investigate their underlying physical basis, and we thus construct a more robust (though still uncertain) framework for extrapolation. For the most part, our results are in agreement with those of Pinzke et al. (2011), but here we also present an estimate of the expected signal-to-noise of the annihilation radiation from nearby clusters and compare it to that from nearby dwarf and giant galaxies.

The outline of our paper is as follows. Sections 2 and 3 give brief descriptions of our simulation suite and of a model for calculating the annihilation flux and its signal-to-noise in an idealised experiment. In Section 4, we discuss our results and their implications for dark matter detection.

2 NUMERICAL SIMULATIONS

The dark matter simulations analysed in this study come from the Phoenix (Gao et al. 2011, in preparation) and Aquarius Projects. The latter is described in Springel et al. (2008a,b). For the Phoenix Project, we have carried out a suite of extremely high resolution simulations of the dark matter distribution in galaxy clusters. This suite consists of nine cluster-size dark matter haloes with masses in the range $[5-20]\times10^{14}\,h^{-1}\mathrm{M}_{\odot}$. These were selected at random from the Millennium Simulation (MS: Springel et al. 2005) and resimulated at various numerical resolutions. The cosmological parameters adopted are those of the original MS and of the Aquarius Project: $\Omega_m=0.25$, $\Omega_\Lambda=0.75$, $\sigma_8=0.9$, $n_s=1$, and a Hubble constant $H_0=100\,h\,\mathrm{km\,s^{-1}}=73\,\mathrm{km\,s^{-1}Mpc^{-1}}$. These were close to the best fit values derived from the first year of data from the WMAP satellite (Spergel et al. 2003) but are not consistent with the parameter ranges found through analysis of the seven-year WMAP data together with other large-scale structure observations (Komatsu et al. 2011). The small offset is, however, of no consequence for the topics addressed in this paper.

The largest of these "Phoenix" simulations, labelled Ph-A-1, represents the dark matter with more than a billion particles within r_{200}, the radius at which the enclosed mean density is 200 times the cosmic critical density. It has a particle mass of $6.4\times10^5h^{-1}\mathrm{M}_{\odot}$ and a Plummer-equivalent force softening of $0.15h^{-1}$kpc in comoving coordinates at all times. This particular cluster has also been simulated at four lower resolution levels (producing Ph-A-2 to Ph-A-5) in order to assess how resolution affects inferences about cluster structure. At the next-to-highest resolution level ($\sim1.3\times10^8$ particles within r_{200}), we have simulated an additional eight clusters (Ph-B-2 to Ph-I-2) with a particle mass of about $5\times10^6h^{-1}\mathrm{M}_{\odot}$ and a force softening of $0.32h^{-1}$kpc in order to quantify the cluster-to-cluster variation in dark matter properties. We will present details of the Phoenix simulation suite in a forthcoming paper (Gao et al. 2011, in preparation).

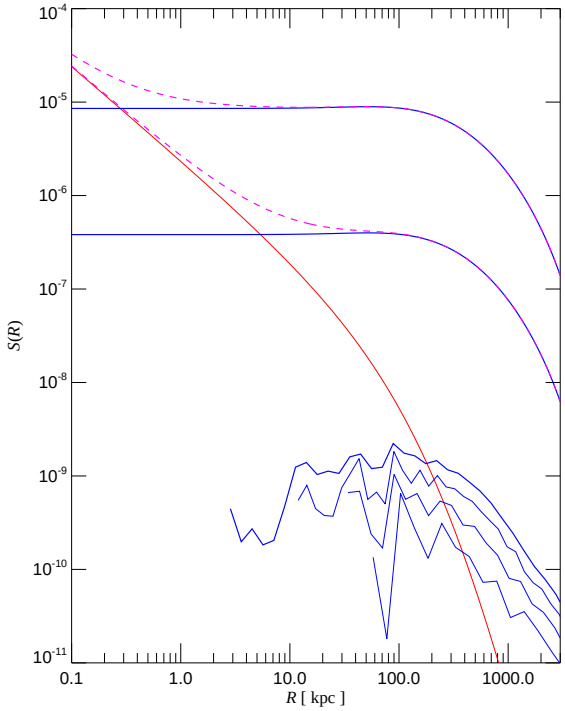

Figure 1. Surface brightness profiles from dark matter annihilation for various components of the Ph-A-1 simulation of a rich galaxy cluster. Surface brightness is given in units of annihilation photons per cm^2 per second per steradian for fiducial values of 100 Gev for m_p, the dark matter particle mass, and $3\times10^{-26}\mathrm{cm^3s^{-1}}$ for $\langle\sigma v\rangle$, the thermally averaged velocity-weighted annihilation cross section, assuming $N_\gamma=2$ photons per annihilation. This surface brightness scales as $N_\gamma\langle\sigma v\rangle/m_p^2$. Projected radius is given in units of kpc. The red line shows radiation from the smoothly distributed dark matter within the main component of the cluster. The ragged blue lines show radiation from resolved dark matter subhaloes with masses exceeding 5×10^7, 5×10^8, 5×10^9 and $5\times10^{10}\,\mathrm{M}_{\odot}$ (from top to bottom). Extrapolating to mass limits of 10^{-6} and $10^{-12}\,\mathrm{M}_{\odot}$ as discussed in the text gives rise to the smooth blue curves. The purple dashed lines show the results of summing smooth and subhalo contributions.

3 RESULTS

3.1 The total cluster surface brightness

The total γ-ray annihilation luminosity of a dark matter halo is the sum of contributions from the smooth main halo, from resolved subhaloes, and from unresolved subhaloes. (Caustics and tidal streams make a negligible contribution to the annihilation luminosity;Vogelsberger & White (2011).) If the density distribution in the inner regions of the smooth main halo and the resolved subhaloes are assumed to be adequately fit by the NFW formula (Navarro et al. 1996, 1997) their emission integrals $\int\rho^2dV$ can be estimated simply as $1.23V_{\mathrm{max}}^4/(G^2r_{\mathrm{max}})$ (Springel et al. 2008a). Here V_{max} is the maximum circular velocity of the halo/subhalo and r_{max} the radius at which this maximum circular velocity is reached.

In Figure 1, we show the azimuthally averaged surface brightness profile for Ph-A-1, split into the components due to the smooth dark matter distribution and to subhaloes resolved down to four mass thresholds differing by factors of ten. The subhalo component is clearly much less centrally concentrated to the cluster centre than the smooth component and its shape appears independent of mass

threshold as far as can be judged given the noise introduced by the finite number of subhaloes involved. The overall level of subhalo emission increases steadily as the threshold decreases. The smallest subhaloes resolved in Ph-A-1 have masses $\sim 5\times10^7\,\mathrm{M}_\odot$, well below the masses expected for the haloes of luminous galaxies but far above the lower limit for subhaloes in a ΛCDM universe which could be as low as $10^{-12}\,\mathrm{M}_\odot$ (Hofmann et al. 2001; Bertone et al. 2005). Considerable extrapolation is thus necessary in order to estimate the total subhalo emission. Note that even at the Ph-A-1 resolution threshold of $5\times10^7\,\mathrm{M}_\odot$, the surface brightness is dominated by the subhalo component at radii greater than 200 kpc.

To calibrate the extrapolation to lower subhalo masses we combine results from our nine Phoenix simulations with results from six higher resolution simulations of galaxy haloes from the Aquarius Project (Springel et al. 2008a,b). Figure 2 shows the total annihilation luminosity per unit halo mass (M_{200}) and per decade in subhalo mass from subhaloes with masses ranging over 7 orders of magnitude, from 10^5 to $10^{12}\,\mathrm{M}_\odot$. In the overlap region between 10^8 and $10^9\,\mathrm{M}_\odot$, the Phoenix and Aquarius results agree to about 30%. This is within the scatter expected given the finite number of realizations (illustrated by the shaded area) and the roll-off as subhalo mass approaches 1% of the parent mass. Well away from these cutoffs, the shape of this curve is very similar to that of the halo luminosity per unit mass expected for the Universe as a whole, shown as the dashed magenta curve in Figure 2. This reflects the fact that the luminosity is dominated by subhaloes in the outer regions which were accreted recently (Gao et al. 2004) and so have similar luminosities and abundance per unit mass (apart from a small bias correction of 1.5) as the haloes in a representative volume of the Universe. Thus, we can use analytic predictions for the abundance and concentration of field haloes (Sheth & Tormen 2002; Neto et al. 2007) to extrapolate our simulation results to much lower subhalo masses. The upper blue curves in Figure 1 show the resulting predictions for minimum subhalo masses of 10^{-6} and $10^{-12}\,\mathrm{M}_\odot$, respectively. The most uncertain part of this extrapolation is the assumption that halo concentration continues to increase towards lower masses in the same way as measured over the mass range simulated so far. This assumption has not yet tested explicitly, and has a very large effect on the results. For example, if all (sub)haloes less massive than $10^5\,\mathrm{M}_\odot$ are assumed to have similar concentration, then the total predicted emission from subhaloes would be more than two orders of magnitude below that plotted in Figure 2 for an assumed cut-off mass of $10^{-6}\,\mathrm{M}_\odot$.

With our adopted concentration scaling, subhaloes dominate the surface brightness beyond projected radii of a few kiloparsecs. Surface brightness is almost constant between 10 and 300 kpc, dropping by a factor of two only at 460 kpc. At the virial radius of the cluster ($r_{200}=1936$ kpc), the surface brightness of the subhalo component is a factor of 14 below its central value. Within this radius the luminosity from resolved subhaloes in Ph-A-1 is almost twice that from the smooth halo, even though these subhaloes account only for 8% of the mass. Extrapolating to minimum subhalo masses of 10^{-6} and $10^{-12}\,\mathrm{M}_\odot$ the subhalo excess becomes 718 and 16089 respectively. These boost factors substantially exceed the equivalent factors predicted for the galaxy haloes of the Aquarius Project. This is a consequence of the additional high-mass subhaloes which contribute in the cluster case (see Figure 2) together with the lower concentration of cluster haloes relative to galaxy haloes, which reduces the emission from the smooth component. Note, the boost factor for the Aq-A-1 obtained with the extrapolation we use here is smaller by a factor of 2.4 than the value quoted in Springel et al. (2008a).

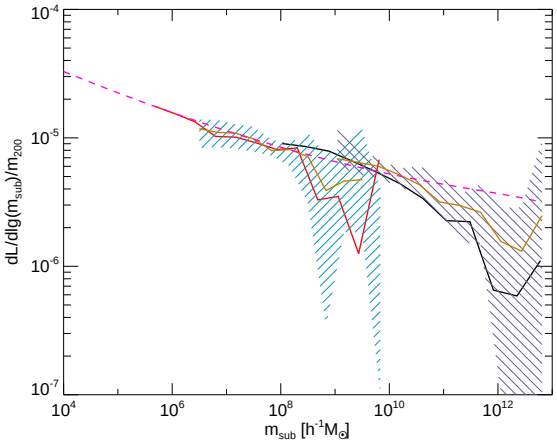

Figure 2. Annihilation luminosity from subhaloes lying within r_{200} per decade in subhalo mass and per unit halo mass (M_{200}) for the Phoenix and Aquarius simulations. The level-1 simulations are shown by the black and red lines and the medians of the nine Phoenix and six Aquarius level-2 simulations by the orange lines. The full scatter in each set of simulations is indicated by the shaded areas. The dashed magenta line gives the predicted annihilation luminosity density per decade in halo mass from the cosmic population of dark matter haloes.

For the resolved component, there is significant variation amongst the nine Phoenix haloes, but the median value of the total boost factor (for a cutoff mass of $10^{-6}M_\odot$) is 1125, which is about twelve times the median boost factor we obtain by applying the same method to the Aquarius haloes by Springel et al. (2008a). Comparing these results suggests that the ratio of subhalo to smooth main halo luminosity within r_{200} (subhalo "boost factor") varies with halo mass approximately as

$$b(M_{200}) = L_{\rm sub}/L_{\rm main} = 1.6\times10^{-3}(M_{200}/\mathrm{M}_\odot)^{0.39}. \quad (1)$$

The total luminosity of a halo is therefore $L_{\rm tot} = (1+b)L_{\rm main}$, where $L_{\rm main}$ is the emission of the smooth halo. In addition, the projected luminosity profile of the subhalo component can be well approximated by

$$S_{\rm sub}(r) = \frac{16b(M_{200})L_{\rm main}}{\pi\ln(17)}\frac{1}{r_{200}^2+16r^2}. \quad (2)$$

These formulae will be used to estimate dark matter annihilation luminosities and surface brightness profiles for haloes with different masses in subsequent sections.

3.2 Surface brightness and signal to noise of galaxies and clusters

Putting together results from the Phoenix and Aquarius projects, we can assess the relative ease of detection of cluster, galaxy and dwarf satellite haloes. In the left panel of Figure 3, we show predicted surface brightness profiles for three of the most promising candidates, the Coma cluster of galaxies, the Andromeda Nebula (M31) and the dwarf satellite galaxy, Ursa Major-II (UMa-II), assuming a minumum subhalo mass of $10^{-6}\,\mathrm{M}_\odot$. We represent Coma and M31 by scaling Ph-A-1 and Aq-A-1 to the appropriate virial masses, $M_{200}=1.3\times10^{15}\,\mathrm{M}_\odot$ (Reiprich & Böhringer 2002) and $1.8\times10^{12}\,\mathrm{M}_\odot$ (Li & White 2008) respectively. We model UMa-II as in Springel et al. (2008a) (including the contribution from substructures – the 'subsub' component). At projected radii below 2

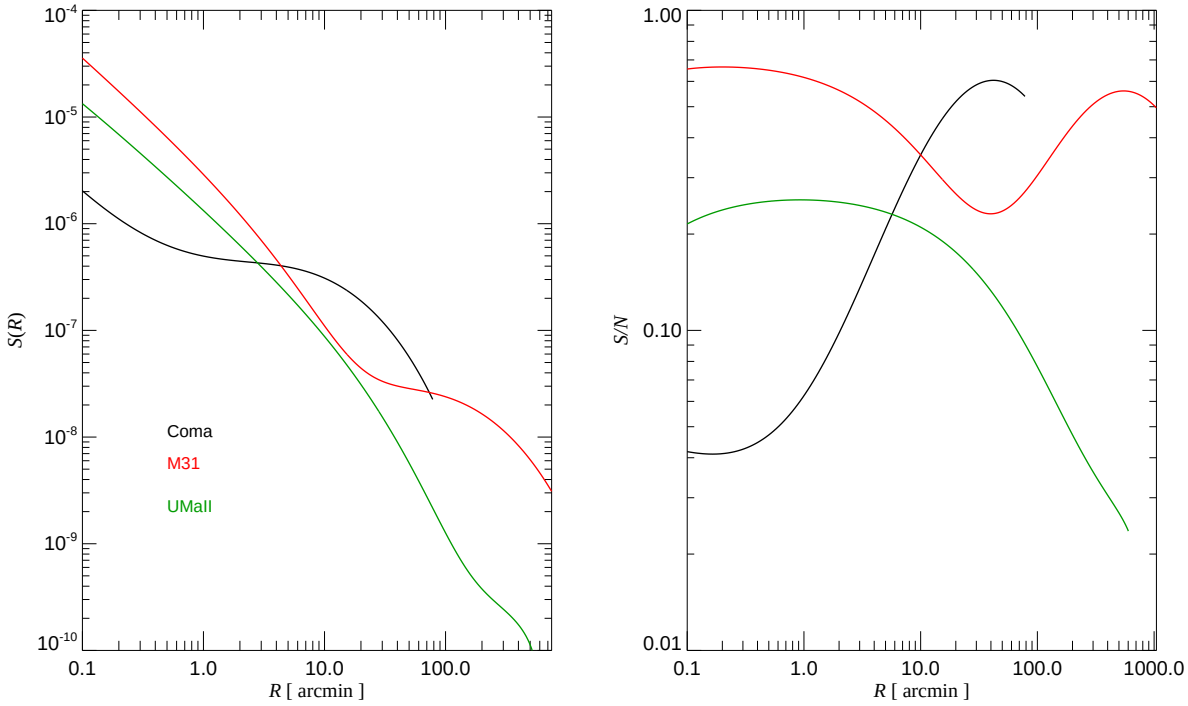

Figure 3. *Left panel:* Predicted surface brightness profiles of annihilation radiation (in units of annihilation photons per cm^2 per second per steradian) for a dwarf galaxy (UMaII; green line), for the nearest large galaxy (M31; red line) and for a rich galaxy cluster (the Coma cluster; black line). As in Figure 1, surface brightness scales as $N_\gamma\langle\sigma v\rangle/m_p^2$. Projected radius is given in arc minutes. The inner steeply rising part of each curve is due to smoothly distributed dark matter in the main halo, while the shoulder of extended emission is produced by low-mass subhaloes. Each profile is truncated at r_{200}, the nominal radius of the dark matter halo. *Right panel:* Estimates of the signal-to-noise ratio within a circular aperture of radius R (in arc minutes). The signal is obtained by direct integration of the corresponding curves in the left-hand panel and the noise is obtained as discussed in the text. S/N scales as $N_\gamma B^{-1/2}\langle\sigma v\rangle/m_p^2$, where B is the surface brightness of the background.

arcmin, M31 is about twice as bright as UMa-II and both are substantially brighter than Coma. However, at 20 arcmin the surface brightness of Coma exceeds that of M31 by a factor of 4 and that of UMa-II by about a factor of 6. Beyond about 60 arcmins, M31 is again the brightest object.

For γ-ray telescopes like Fermi, the detectability of extended objects depends on their contrast relative to the diffuse background. As a simple indicator of signal-to-noise (S/N), in the right panel of Figure 3 we estimate the signal within a circular aperture from the enclosed luminosity, and the noise as the square root of the background counts, assumed to be $B\times A\times t$, where B is the background count rate per unit area, A is the area of the aperture in square arc minutes, and t is the exposure time. (This assumes that the background is larger than the signal which may not be the case for the smallest apertures.) For the dwarf galaxy UMa-II, the effective S/N is almost independent of aperture for radii less than 10 arcmin, but drops dramatically at larger radii. In contrast, the S/N for Coma rises steeply with increasing aperture to a peak at a radius of about 30 arcmin, significantly larger than the few arcmin resolution of the Fermi Large Area Telescope (LAT) at energies ~ 10 GeV. For M31, the effective S/N has a minimum on this scale and has maxima on scales of one and 300 arcmin. In this simple set-up the maximum achievable S/N ratios for Coma and M31 exceed that for UMa-II by about a factor of 3.

In practice, realistic experiments will find it difficult to achieve these theoretical S/N values for very large apertures. Systematic effects due to variable backgrounds and difficulties in masking bright sources make background correction significantly easier for small apertures. M31 is a particularly difficult case because of its very large angular size, its low galactic latitude, and confusion from other γ-ray sources in its inner regions. The Coma cluster is significantly more promising because it lies close to the North Galactic Pole and appears 10 times smaller on the sky. On the other hand, an overly small aperture, corresponding for example to the few arcmin resolution of the Fermi LAT instrument at about 10 GeV, would miss a large fraction of the signal in Coma and other nearby galaxy clusters. For a uniform background, the optimal filter has the same shape similar to the predicted profile (Springel et al. 2008a) shown in Figure 3 and represented by equation (2).

4 DISCUSSION AND CONCLUSION

In Table 1 we summarise properties of some nearby astronomical objects which are relevant for the detectability of their dark matter annihilation signal. We consider six galaxy clusters which were already analyzed by the Fermi collaboration (Ackermann et al. 2010), thirteen of the known dwarf satellites of our Galaxy, and the nearest giant galaxy, M31.

For the galaxy clusters, distances were taken from the NASA/IPAC Extragalactic Database[1], and virial masses M_{200} (based on X-ray data) from Reiprich & Böhringer (2002). Values

[1] http://nedwww.jpac.caltech.edu/

Object Name	Half-light radius [arcmin]	Distance [Mpc]	M_{200} [$M_\odot$]	L [$L_{\rm mw}$]	$F = L/(4\pi d^2)$ [$F_{\rm mw}$]	S/N [$(S/N)_{\rm mw}$]
AWM 7	35.5	67.0	4.2×10^{14}	7.1×10^{4}	3.2×10^{-4}	6.8×10^{-3}
Fornax Cluster	84.1	17.5	1.0×10^{14}	1.2×10^{4}	8.0×10^{-4}	7.3×10^{-3}
M49	59.6	18.2	0.4×10^{14}	3.9×10^{3}	2.4×10^{-4}	3.1×10^{-3}
NGC 4636	52.6	17.4	0.24×10^{14}	2.1×10^{3}	1.4×10^{-4}	2.0×10^{-3}
Centaurus (A3526)	40.1	50.5	2.6×10^{14}	3.9×10^{4}	3.1×10^{-4}	5.8×10^{-3}
Coma	36.1	95.8	1.3×10^{15}	2.9×10^{5}	6.4×10^{-4}	1.3×10^{-2}
Draco	16.4	0.082	N/A	5.2×10^{-3}	1.6×10^{-5}	6.3×10^{-4}
UMaI	18.4	0.066	N/A	4.3×10^{-3}	2.0×10^{-5}	7.5×10^{-4}
LeoI	4.4	0.25	N/A	3.5×10^{-3}	1.2×10^{-6}	8.2×10^{-5}
Fornax dwarf	5.9	0.138	N/A	2.0×10^{-3}	2.2×10^{-6}	1.5×10^{-4}
LeoII	2.5	0.205	N/A	8.5×10^{-4}	4.1×10^{-7}	3.1×10^{-5}
Carina	4.6	0.101	N/A	7.1×10^{-4}	1.4×10^{-6}	1.0×10^{-4}
Sculpt	13.2	0.079	N/A	3.2×10^{-3}	1.0×10^{-5}	4.9×10^{-4}
Sext	3.3	0.086	N/A	3.0×10^{-4}	8.3×10^{-7}	6.1×10^{-5}
UMaII	28.8	0.032	N/A	2.6×10^{-3}	5.2×10^{-5}	1.3×10^{-3}
Comber	15.9	0.044	N/A	1.6×10^{-4}	1.7×10^{-5}	6.8×10^{-4}
WilI	17.7	0.066	N/A	3.9×10^{-3}	1.8×10^{-5}	7.0×10^{-4}
LMC	82.5	0.049	N/A	3.8×10^{-2}	3.3×10^{-4}	3.1×10^{-3}
SMC	45.5	0.061	N/A	1.9×10^{-2}	1.1×10^{-4}	1.8×10^{-3}
M31	351.5	0.807	1.8×10^{12}	1.3×10^{2}	4.2×10^{-3}	9.3×10^{-3}

Table 1. Principal properties of nearby galaxy clusters, prominent satellites of the Milky Way, and the Andromeda Nebula, M31. The annihilation luminosity, L, is given in units of the luminosity from the smooth component of the main Aq-A halo, which we use as a proxy for the Milky Way. The observed flux, F, is expressed relative to the flux received by an observer placed 8 kpc from the centre of Aq-A. Similarly, the predicted S/N for an optimal filter placed on each object is normalized to the signal-to-noise predicted for a similar filter tuned to the diffuse emission of Aq-A seen from this observer location. For the signal-to-noise calculations, we use the optimal filter of Springel et al. (2008a) assuming the background to be the same everywhere and to dominate the signal in all objects.

for $V_{\rm max}$ and $r_{\rm max}$ were derived assuming an NFW density profile (Navarro et al. 1996, 1997) and the mass concentration relation of Neto et al. (2007). We have verified that this relation is consistent with our simulation data down to the resolution limit of Aq-A-1, which is about $10^5\,M_\odot$.

Data for dwarf satellites were taken from the mass models of Peñarrubia et al. (2008). Their γ-ray luminosities are estimated from an emission integral based on the NFW formula, $\int \rho^2 dV = 1.23 V_{\rm max}^4/(G^2 r_{\rm max})$. As discussed in Springel et al. (2008a), the annihilation signal due to substructures within Milky Way dwarfs (the 'subsub' component) is less than that due to the smooth component of their haloes in almost all cases, so we do not consider it here. The distance of M31 was also taken from the NASA/IPAC Extragalactic Database. We base structural parameters for the M31 halo on the Aq-A-1 simulation which has a very similar mass (Li & White 2008).

We estimate a "best case" signal-to-noise for each object using the optimal filter discussed by Springel et al. (2008a) and assume a uniform background accross the whole sky which dominates over the signal in all objects. In this case, the optimal filter has the same shape as the signal, and the signal-to-noise can be written in the generic form

$$S/N = f_{\rm shape}(\theta_h/\theta_{\rm psf}) \left[\frac{tA_{\rm eff}}{B}\right]^{1/2} \frac{F}{(\theta_h^2+\theta_{\rm psf}^2)^{1/2}}, \qquad (3)$$

where $F = L/(4\pi d^2)$ is the photon flux, θ_h the half-light radius, $\theta_{\rm psf}$ ($\simeq 10$ arcmin for Fermi at the relevant energies (Michelson 2007)) describes the point spread function of the instrument, t is the integration time, $A_{\rm eff}$ is the effective collecting area of the telescope, and B is the background count rate per unit solid angle. The function $f_{\rm shape}(x)$ encodes the detailed shape (Springel et al. 2008a) of the emission profile of the signal; it is of order unity and depends only weakly on the ratio $x = \theta_h/\theta_{\rm psf}$.

Using the techniques discussed above, we can compare the apparent γ-ray luminosities and achievable S/N ratios for galaxy clusters with those estimated by Springel et al. (2008a) for dwarf satellites of the Milky Way. Results are shown in the Table. We find that the brightest nearby cluster, Fornax, is predicted to appear 15 times more luminous than the brightest dwarf spheroidal, UMaII, and 40-50 times more luminous than UMaI, Draco or the ultrafaint satellite, Wilman-1. However, the Fornax cluster is quite extended on the sky, and, as a result, when optimal filters are used, the slightly fainter but more compact Coma cluster has a predicted S/N ratio 1.8 times larger and ten times that of the most easily detectable dwarf spheroidal, UMaII. Although the Andromeda Nebula is predicted to have comparable S/N, it is not a promising target because of the difficulty in correcting for foreground and other sources of emission. Note that the S/N predicted for both objects is still very small compared to that of the main component of the Milky Way's smooth halo. Here also, of course, the main problem is in separating annihilation radiation from other γ-ray signals.

The Coma cluster thus offers an order of magnitude better opportunity than any Milky Way satellite for detecting dark matter or placing limits on its annihilation cross-section. As we have shown, for a high resolution experiment like Fermi, the sensitivity for detecting such radiation will be enhanced by use of a filter which is properly matched to the expected extent of the object. For example, for the optimal filter, the S/N expected for Coma is about 1.5 times higher than the S/N for a filter based on the point-spread function

of the Fermi LAT, assuming 10 arcmin for the latter at the relevant energies. Detecting annihilation radiation from the Coma or Fornax clusters or the placing of robust and stringent upper limits will also require careful subtraction of astrophysical sources and an accurate estimate of the background.

ACKNOWLEDGEMENTS

We thank the Supercomputer Center of the Chinese Academy of Science, where the simulations were carried out. LG acknowledges support from the one-hundred-talents program of the Chinese academy of science(CAS), the National basic research program of China (973 program under grant No. 2009CB24901), the NSFC grants program (No. 10973018), the Partner Group program of the Max Planck Society, and an STFC Advanced Fellowship, as well as the hospitality of the Institute for Computational Cosmology in Durham, UK. CSF acknowledges a Royal Society Wolfson Research Merit Award and ERC Advanced Investigator grant COSMIWAY. This work was supported in part by an STFC rolling grant to the ICC.

REFERENCES

Abdo A. A., Ackermann M., Ajello M., et al., 2010, ApJ, 712, 147
Ackermann M., Ajello M., Allafort A., et al., 2010, JCAP, 5, 25
Anderson B., Kuhlen M., Diemand J., Johnson R. P., Madau P., 2010, ApJ, 718, 899
Berezinsky V., Bottino A., Mignola G., 1994, Physics Letters B, 325, 136
Berezinsky V., Dokuchaev V., Eroshenko Y., 2003, Phys. Rev. D, 68, 10, 103003
Bergström L., Ullio P., Buckley J. H., 1998, Astroparticle Physics, 9, 137
Bertone G., Hooper D., Silk J., 2005, Physics Reports, 405, 279
Colafrancesco S., Profumo S., Ullio P., 2007, Phys. Rev. D, 75, 2, 023513
Diemand J., Kuhlen M., Madau P., 2007, ApJ, 657, 262
Diemand J., Kuhlen M., Madau P., et al., 2008, Nat, 454, 735
Gao L., White S. D. M., Jenkins A., Stoehr F., Springel V., 2004, MNRAS, 355, 819
Green A. M., Hofmann S., Schwarz D. J., 2005, JCAP, 8, 3
Hofmann S., Schwarz D. J., Stöcker H., 2001, Phys. Rev. D, 64, 8, 083507
Jeltema T. E., Kehayias J., Profumo S., 2009, Phys. Rev. D, 80, 2, 023005
Kamionkowski M., Koushiappas S. M., Kuhlen M., 2010, Phys. Rev. D, 81, 4, 043532
Komatsu E., Smith K. M., Dunkley J., et al., 2011, ApJS, 192, 18
Koushiappas S. M., Zentner A. R., Walker T. P., 2004, Phys. Rev. D, 69, 4, 043501
Kuhlen M., Diemand J., Madau P., 2008, ApJ, 686, 262
Li Y.-S., White S. D. M., 2008, MNRAS, 384, 1459
Michelson P. F., 2007, in The First GLAST Symposium, edited by S. Ritz, P. Michelson, & C. A. Meegan, vol. 921 of American Institute of Physics Conference Series, 8–12
Navarro J. F., Frenk C. S., White S. D. M., 1996, ApJ, 462, 563
Navarro J. F., Frenk C. S., White S. D. M., 1997, ApJ, 490, 493
Neto A. F., Gao L., Bett P., et al., 2007, MNRAS, 381, 1450
Peñarrubia J., Navarro J. F., McConnachie A. W., 2008, ApJ, 673, 226
Pieri L., Bertone G., Branchini E., 2008, MNRAS, 384, 1627
Pinzke A., Pfrommer C., Bergstrom L., 2011, ArXiv:1105.3240
Reiprich T. H., Böhringer H., 2002, ApJ, 567, 716
Sheth R. K., Tormen G., 2002, MNRAS, 329, 61
Spergel D. N., Verde L., Peiris H. V., et al., 2003, ApJS, 148, 175
Springel V., White S. D. M., Frenk C. S., et al., 2008a, Nat, 456, 73
Springel V., Wang J., Vogelsberger M., et al., 2008b, MNRAS, 391, 1685
Springel V., White S. D. M., Jenkins A., et al., 2005, Nat, 435, 629
Stoehr F., White S. D. M., Springel V., Tormen G., Yoshida N., 2003, MNRAS, 345, 1313
Strigari L. E., Koushiappas S. M., Bullock J. S., et al., 2008, ApJ, 678, 614
Vogelsberger M., White S. D. M., 2011, MNRAS, 413, 1419
Zavala J., Springel V., Boylan-Kolchin M., 2010, MNRAS, 405, 593